A novel method for determination of aragonite saturation state on the continental shelf of central Oregon using multi-parameter relationships with hydrographic data

L. W. Juranek,[1] R. A. Feely,[1] W. T. Peterson,[2] S. R. Alin,[1] B. Hales,[3] K. Lee,[4] C. L. Sabine,[1] and J. Peterson[5]

Received 3 September 2009; revised 10 November 2009; accepted 23 November 2009; published 31 December 2009.

[1] We developed a multiple linear regression model to robustly determine aragonite saturation state (Ω_{arag}) from observations of temperature and oxygen ($R^2 = 0.987$, RMS error 0.053), using data collected in the Pacific Northwest region in late May 2007. The seasonal evolution of Ω_{arag} near central Oregon was evaluated by applying the regression model to a monthly (winter)/bi-weekly (summer) water-column hydrographic time-series collected over the shelf and slope in 2007. The Ω_{arag} predicted by the regression model was less than 1, the thermodynamic calcification/dissolution threshold, over shelf/slope bottom waters throughout the entire 2007 upwelling season (May–November), with the $\Omega_{arag} = 1$ horizon shoaling to 30 m by late summer. The persistence of water with $\Omega_{arag} < 1$ on the continental shelf has not been previously noted and could have notable ecological consequences for benthic and pelagic calcifying organisms such as mussels, oysters, abalone, echinoderms, and pteropods. **Citation:** Juranek, L. W., R. A. Feely, W. T. Peterson, S. R. Alin, B. Hales, K. Lee, C. L. Sabine, and J. Peterson (2009), A novel method for determination of aragonite saturation state on the continental shelf of central Oregon using multi-parameter relationships with hydrographic data, *Geophys. Res. Lett.*, *36*, L24601, doi:10.1029/2009GL040778.

1. Introduction

[2] Since the preindustrial, atmospheric loading of CO_2 from fossil fuel combustion and land use changes has driven an anthropogenic ocean uptake of 146 ± 20 Pg C (updated from *Sabine and Feely* [2007]) and a corresponding average surface water *p*H change of 0.1 units [*Feely et al.*, 2004]. Accelerating emission rates and reduced buffering capacity will decrease *p*H by as much as 0.3–0.4 units by the end of this century under business-as-usual scenarios [*Orr et al.*, 2005]. Effects of these "ocean acidification" changes on marine organisms are still under intense study [*Kleypas et al.*, 2006; *Fabry et al.*, 2008; *Doney et al.*, 2009], but increased ocean CO_2 content will result in a reduced saturation state for calcium carbonate minerals and potentially deleterious impacts for organisms that form $CaCO_3$ shells, including corals, pteropods, foraminifera, and commercially important shellfish and their larvae.

[3] The saturation state (Ω) of $CaCO_3$ minerals is determined by the relationship:

$$\Omega = \left[Ca^{2+}\right]\left[CO_3^{2-}\right]/K'_{sp}, \quad (1)$$

where K'_{sp}, the stoichiometric solubility product, is a function of temperature, salinity, pressure, and the particular mineral phase (aragonite or calcite). In a thermodynamic sense, $\Omega > 1$ indicates mineral precipitation is favored and $\Omega < 1$ indicates dissolution is favored, although biogenic calcification is subject to "vital effects" such as organic shell coatings and species-specific calcification mechanisms, and calcification/dissolution can occur when ambient-water Ω values indicate opposing thermodynamic effects [*Langdon et al.*, 2003; *Tunnicliffe et al.*, 2009]. However, recent experiments indicate that $\Omega < 1$ adversely impacts some organisms; *Fabry et al.* [2008] reported net dissolution in live pteropods within 48 hours of exposure to undersaturated water. Because aragonitic $CaCO_3$ has a metastable crystalline structure and is ≈50% more soluble than calcite [*Mucci*, 1983], organisms that form aragonitic shells will likely be affected first, and perhaps most severely, by ocean acidification.

[4] Transient episodes of reduced aragonite Ω (Ω_{arag}) have already been noted in productive eastern boundary upwelling systems such as the California current system [*Feely et al.*, 2008a]. Understanding the duration, intensity, and overall ecological impact of these events is a key need in economically and socially important coastal fisheries regions. Here we present an approach, updated from *Feely et al.* [2008b], to determine Ω_{arag} from temperature and O_2, using data collected on a 2007 survey of North American Pacific coastal waters. We justify the approach with a statistical evaluation, and apply it to a hydrographic time-series from the central Oregon coast to evaluate seasonal changes in Ω_{arag}.

2. Algorithm Development

[5] Ω_{arag} is a function of temperature (T), salinity (S), pressure (P), and the $[Ca^{2+}]$ and $[CO_3^{2-}]$ of seawater (equation (1)). Because $[Ca^{2+}]$ changes are proportionally small in seawater, variations in Ω_{arag} are largely determined by changes in $[CO_3^{2-}]$, which can be predicted from observations of dissolved inorganic carbon (DIC) and total

[1]Pacific Marine Environmental Laboratory, NOAA, Seattle, Washington, USA.
[2]Northwest Fisheries Science Center, NMFS, Newport, Oregon, USA.
[3]College of Oceanic and Atmospheric Sciences, Oregon State University, Corvallis, Oregon, USA.
[4]School of Environmental Science and Engineering, Pohang University of Science and Technology, Pohang, South Korea.
[5]Cooperative Institute for Marine Resources Studies, Oregon State University, Newport, Oregon, USA.

0094-8276/09/2009GL040778

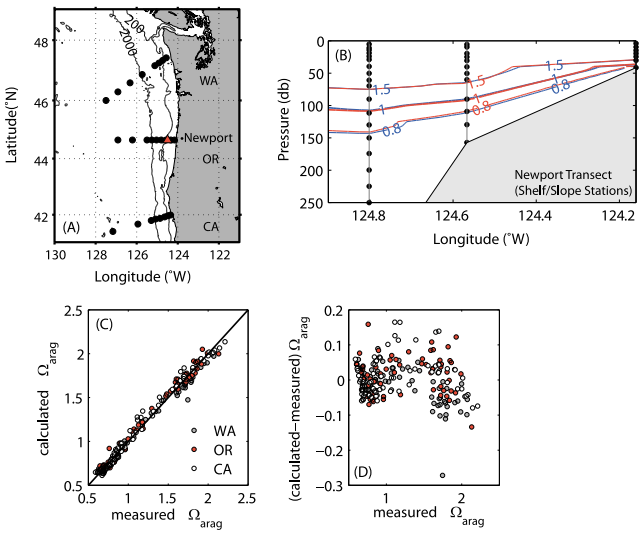

Figure 1. (a) Region map showing location of three coastal transects used in developing the algorithm and location of NDBC buoy 46050 (red triangle). Sampling locations for the Newport time-series shown in Figure 2 are similar to those shown here, but with higher resolution over shelf/slope areas and a reduced seaward extent. (b) Ω_{arag} (blue) and Ω^{e}_{arag} (red) contours for transect collected near Newport, Oregon in late May 2007, with profiles (vertical lines) and sampling depths indicated. (c) Measured Ω_{arag} and calculated Ω^{e}_{arag}, color coded by transect location. Lack of geographic bias in residuals indicates that the algorithm applies for WA, OR, and N. CA coastal areas. (d) Residual ($\Omega^{e}_{arag} - \Omega_{arag}$) versus Ω_{arag} for PNW data, color coded as in C. All Ω^{e}_{arag} values were determined using the regression model described by equation (3).

alkalinity (TA). DIC concentrations are governed by physics (solubility, surface gas exchange) and biology (photosynthesis/respiration) and therefore should be a function of T, S, and either O_2 or NO_3^- [*Anderson and Sarmiento*, 1994; *Lee et al.*, 2000]. TA can also be modeled as a function of T and S [*Lee et al.*, 2006]. We would therefore expect a predictive relationship for Ω_{arag} as a function of T, S, P, O_2, NO_3^-, or a subset of these parameters.

[6] A hydrographic survey of the U.S. west coast in 2007 [*Feely et al.*, 2008a] allowed an opportunity to develop predictive relationships for Ω_{arag} based on contemporaneous T, S, P, O_2, and NO_3^- measurements. We first evaluated a linear additive model of the following form:

$$\Omega^{e}_{arag} = \beta_0 + \beta_1 T + \beta_2 S + \beta_3 P + \beta_4 O_2 + \beta_5 NO_3^-, \qquad (2)$$

where Ω^{e}_{arag} is the empirically predicted aragonite saturation state, and the coefficients β_i are empirical constants. We determined coefficients for equation (2) using an ordinary least-squares regression of Ω_{arag} observations collected in the Pacific Northwest (PNW) region (transects of Washington, Oregon, and N. California coastal waters, Figure 1a), using only data in the 30–300 m depth range to minimize localized effects of surface warming, gas exchange and riverine inputs and to include only relevant source water masses for the shelf/slope region. Although all resulting regression coefficients were significant, tests of collinearity among the independent variables (via pair wise regression and the variance inflation factor test, see Table 1) indicated that S, O_2, and NO_3^- were too closely related, leading to potential errors in least-squares regression coefficients [*Kutner et al.*, 2004]. Stepwise regression and regression statistics (R^2, RMS error) subsequently identified O_2 as the most robust predictor of the three collinear variables.

[7] A multiple linear regression of T, P, and O_2 yielded significant regression coefficients and reasonable regression statistics (Table 1). However, residuals for this relationship showed a strong bias, i.e., overestimation of Ω^{e}_{arag} at minimum and maximum T and O_2 (see Figure S1 of the auxiliary material).[1] This bias is likely the result of the non-linear dependence of CO_3^{2-} on TA and DIC, which arises in coastal waters with high pCO_2 and significant contributions to TA from non-carbon species. We examined several possible non-linear terms and found that the bias could be minimized through the addition of an interaction term between T and O_2 (Figure S1); when this term is added, P and T are no longer significant as predictor variables. To reduce large magnitudes of the product of $T \cdot O_2$ and subsequent errors in the least-squares regression analysis (Table 1) [*Kutner et al.*, 2004], we normalized each term by subtracting a reference value for each variable, i.e.,

$$\Omega^{e}_{arag} = \alpha_0 + \alpha_1(O_2 - O_{2,r}) + \alpha_2(T - T_r)\cdot(O_2 - O_{2,r}). \qquad (3)$$

Where α's indicate regression coefficients and T_r and $O_{2,r}$ are values representative of upwelling source water in the PNW region (T_r = 8°C and $O_{2,r}$ = 140 μmol/kg, see Figure 2 and Table 1). The resulting model had improved regression statistics (Table 1) and resulted in Ω^{e}_{arag} predictions that correctly reproduce both the magnitude and depth-distribution of Ω_{arag} observations for the effective range experienced over the shelf/slope areas (≈0.6 to 2.2) of the PNW region (Figure 1).

3. Model Evaluation and Caveats

[8] We evaluated the skill of the model described by equation (3) by comparison of the unexplained error in Ω^{e}_{arag} and the ability to constrain Ω_{arag} given analytical uncertainties in DIC and TA (2 and 3 μmol/kg, respectively [*Feely et al.*, 2008a]). Uncertainty in Ω_{arag} was determined by a Monte Carlo approach, in which DIC and TA inputs into the Matlab® program CO2SYS [*van Heuven et al.*, 2009] were varied randomly about chosen values for the PNW data, with standard deviations equal to analytical uncertainties. The 1σ values of 1000 individually calculated Ω_{arag} determinations, 0.017/0.034 for minimum/maximum Ω_{arag} values in the PNW data (0.61/2.22, respectively), represent the theoretical lower limit for unexplained random error, ε, in any model used to predict Ω^{e}_{arag}. The RMS error determined for the equation (3) model is close to, but still slightly higher than, the limit calculated for analytical uncertainties alone (ε). Although adding new terms to the regression model causes the RMS error to approach ε, the contribution of these additional terms to the explained

[1] Auxiliary materials are available in the HTML. doi:10.1029/2009GL040778.

Table 1. Summary of Model Parameters, Coefficients, and Indicators Used in Model Selection[a]

Parameters	VIF[b]	R^2	RMS Error	Coefficients ± STD Error[c]	Comments
T, S, P, O_2, NO_3^-	3.9, 24, 2.9, 35, 9.3	0.966	0.090	$\beta_0 = 6.3 \pm 1.7$ $\beta_1 = 9.5{\cdot}10^{-2} \pm 1.0{\cdot}10^{-2}$ $\beta_2 = -1.94{\cdot}10^{-1} \pm 5.0{\cdot}10^{-2}$ $\beta_3 = 8.6{\cdot}10^{-4} \pm 1.5{\cdot}10^{-4}$ $\beta_4 = 2.82{\cdot}10^{-3} \pm 4.5{\cdot}10^{-4}$ $\beta_5 = -3.7{\cdot}10^{-3} \pm 1.7{\cdot}10^{-3}$	O_2, S, and NO_3^- collinear (VIF > 5)
T, O_2, P	2.8, 3.8, 3.0	0.965	0.084	$\beta_0 = -0.521 \pm 7.0{\cdot}10^{-2}$ $\beta_1 = 7.74{\cdot}10^{-2} \pm 8.3{\cdot}10^{-3}$ $\beta_2 = 5.18{\cdot}10^{-3} \pm 1.3{\cdot}10^{-4}$ $\beta_3 = 1.16{\cdot}10^{-3} \pm 1.3{\cdot}10^{-4}$	Residuals show bias at high/low O_2 and T (see Figure S1)
O_2	N/A	0.946	0.088	$\beta_0 = 1.145 \pm 6{\cdot}10^{-3}$ $\beta_1 = 4.99{\cdot}10^{-3} \pm 7{\cdot}10^{-5}$	Residuals show bias, as above
$(O_2-O_{2,r})$, $(T-T_r){\cdot}(O_2-O_{2,r})$	**1.5, 1.5**	**0.987**	**0.053**	$\boldsymbol{\alpha_0 = 9.242{\cdot}10^{-1} \pm 4.4{\cdot}10^{-3}}$ $\boldsymbol{\alpha_1 = 4.492{\cdot}10^{-3} \pm 5.0{\cdot}10^{-5}}$ $\boldsymbol{\alpha_2 = 9.40{\cdot}10^{-4} \pm 3.4{\cdot}10^{-5}}$	**T_r = 8°C; $O_{2,r}$ = 140 μmol/kg;**
$(T-T_r)$, $(O_2-O_{2,r})$, $(T-T_r){\cdot}(O_2-O_{2,r})$, $(S-S_r){\cdot}(O_2-O_{2,r})$, $(P-P_r){\cdot}(O_2-O_{2,r})$	9, 33, 7, 23, 19	0.990	0.043	$\alpha_0 = 9.079{\cdot}10^{-1} \pm 4.6{\cdot}10^{-3}$ $\alpha_1 = 3.37{\cdot}10^{-2} \pm 7.0{\cdot}10^{-3}$ $\alpha_2 = 3.4710^{-3} \pm 1.8{\cdot}10^{-4}$ $\alpha_3 = 7.49{\cdot}10^{-4} \pm 5.9{\cdot}10^{-5}$ $\alpha_4 = -1.32{\cdot}10^{-3} \pm 1.3{\cdot}10^{-4}$ $\alpha_5 = 5.8{\cdot}10^{-6} \pm 1.2{\cdot}10^{-6}$	T_r = 8°C; $O_{2,r}$ = 140 μmol/kg; P_r = 200 dbar S_r = 34

[a]Bold denotes selected model. 227 observations used in each model.

[b]VIF: Variance inflation factor. See *Kutner et al.* [2004] for a full description, but briefly, the VIF is an objective measure of the inflation in coefficient uncertainty from poorly scaled or singular matrices (e.g., due to rounding errors during matrix inversion). The VIF is calculated as $(1-R^2)^{-1}$ for the regression of each variable versus the remaining independent variables; values given in the order parameters are listed. Values >5 indicate potential collinearity among predictor variables.

[c]Coefficients with standard error estimates for robust-fit multiple linear regression, which reduces the weight of outliers in the regression analysis. Coefficients correspond to order in which parameters appear. Following equations (2) and (3) in text, β and α values are coefficients for regressions without/with a reference value subtracted.

variance is marginal (Table 1). To avoid overfitting, we rejected these models. A simple model based only on O_2, which was the strongest predictor variable of Ω^e_{arag} (R^2 = 0.946, RMS error 0.088; Table 1) was also considered. However, the O_2 model had a higher RMS error and a strong bias in residuals similar to that observed for the multiple linear regression of T, P, and O_2 (Figure S1). Based on these observations, we chose the equation (3) model.

[9] Because the only Ω_{arag} data available for algorithm development in this region are from late May 2007, we note there may be important caveats to a seasonal application of equation (3). However, three lines of evidence indicate seasonal application is justified. First, biologically-driven changes in Ω_{arag} for the 30–300 m depth range (i.e., due to remineralization of organic matter over the productive summer months) are to a first order driven by changes in DIC rather than TA, since diatoms typically dominate coastal upwelling systems [*Lassiter et al.*, 2006]. DIC and O_2 changes are expected to be proportional in remineralization zones that are not anoxic [*Hales et al.*, 2005; *Anderson and Sarmiento*, 1994], and therefore changes in DIC should be inherently captured in an algorithm involving O_2. Second, the T-S (and T-O_2) range experienced spatially in the PNW data is similar to the range observed seasonally near Newport (see Figure S2), suggesting that the water masses present in the seasonal data are present in the regional PNW data. Finally, algorithm developments for the Southern California Bight region suggest no significant bias of algorithm development using only late May data (i.e., difference of measured and predicted values for August 2008 was 0.075 (S. Alin, unpublished data, 2009)). As more Ω_{arag} data become available, the algorithm for this region can be tested and refined. Nevertheless, these arguments point toward the ability to model the seasonal Ω_{arag} dynamics near Newport with the data in hand.

[10] One potential time frame when algorithm predictions could deviate from observations is between February and May. PNW coastal waters experience intense river inputs during the rainy winter months, and the TA:DIC signature of these freshwaters is often different than in the open ocean [*Park et al.*, 1969]. Proportionality of $[Ca^{2+}]$ to salinity, an assumption used in calculating Ω_{arag}, may also change during these months. Consequently, we do not present predictions for this time period.

4. Seasonal Evolution of Ω^e_{arag} on the Oregon Coast

[11] We calculated the seasonal evolution of Ω^e_{arag} on the shelf and slope near Newport, Oregon with the model described by equation (3) and a time-series of T and O_2 data (described by *Peterson and Keister* [2003]) collected on biweekly to monthly intervals in 2007. The central Oregon coast is located in the northern end of the California Current system and experiences seasonal upwelling during spring and summer months. The region has been well-studied with regard to the physical forcing driving seasonal and interannual variability in water properties (cf. the 2006 *Geophysical Research Letters* special issue devoted to this region). Selected sections of Ω^e_{arag} (Figure 2) show a distinct seasonal cycle that is tightly coupled to upwelling dynamics near Newport. In January, the Ω^e_{arag} = 1 saturation horizon sits near the shelf break (≈125 m), roughly at the depth horizon of the 140 μmol/kg O_2 contour and the

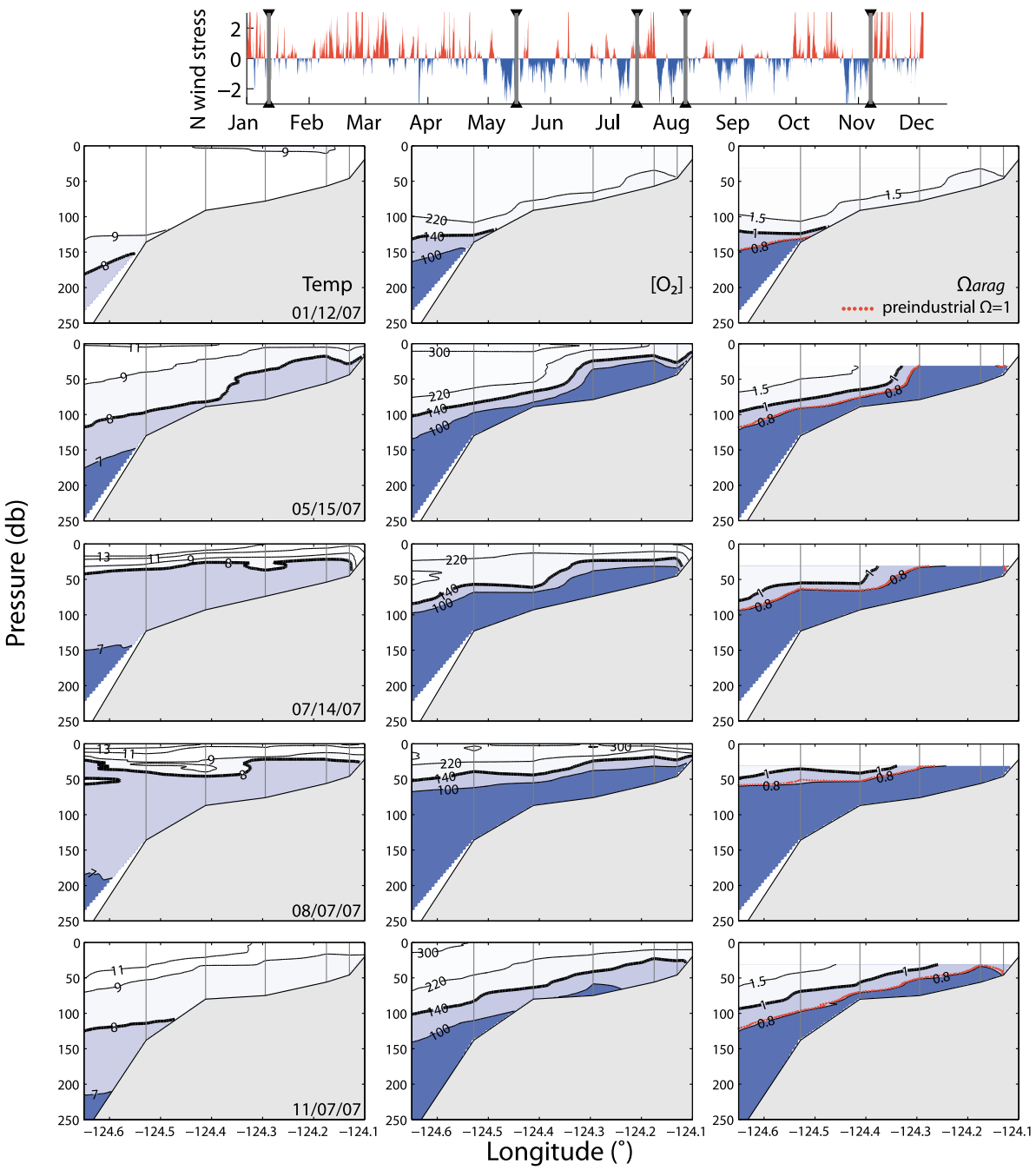

Figure 2. (bottom) Selected sections of T (°C, left), [O_2] (μmol/kg, center), and Ω^e_{arag} (right), for January to November 2007. Ω^e_{arag} was calculated from T and O_2 data (averaged in 1 db bins) using the regression model described by equation (3). Also shown is an estimated preindustrial $\Omega^e_{arag} = 1$ line. Locations of profiles indicated by vertical lines. Note that Ω^e_{arag} are only shown for depths greater than 30 m (see text for explanation). Propagated uncertainty in Ω^e_{arag}, based on uncertainties of T and O_2 data (0.003°C and 0.45 μmol/kg, respectively) is 0.002. (top) Northward wind stress (dynes cm^{-2}) from NDBC buoy 46050 (see Figure 1 for location), with upwelling-favorable winds (southward winds, negative wind stress) denoted in blue and downwelling-favorable winds (northward winds, positive wind stress) denoted in red. Dates of sections are designated by grey bars.

9°C isotherm. The 1.5 Ω^e_{arag} horizon is 25 m shallower, at ≈100 m. The onset of upwelling season begins in early May with the physical spring transition [*Huyer et al.*, 1979], during which wind forcing becomes predominantly equatorward, and offshore transport becomes positive. The offshore transport is compensated by the upwelling of cold, dense waters that are rich in DIC and nutrients, and poor in O_2. The strong upwelling event in mid-May (strongly negative N wind stress, blue lines in Figure 2 (top)) results in sharply up-warped iso-surfaces, and the outcropping of the 0.8 Ω^e_{arag} horizon to the upper 30 m from the mid-shelf (80 m isobath) to the coast. After the spring transition, persistent upwelling-favorable winds pull the 1.0 Ω^e_{arag} and the 140 μmol/kg O_2 contour onto the shelf where they

remain through mid-November (Figure 2). Occasional poleward wind stress events (Figure 2, top) result in relaxation from upwelling, but the source water remains over shelf/slope regions. The late May transect used to formulate the algorithm (Figure 1b) occurred during one of these relaxation events.

[12] Throughout the remainder of the season Ω^e_{arag} and O_2 distribution show depletion on similar hydrographic surfaces, presumably as a result of biological activity (e.g., 1.0/1.5 Ω^e_{arag} and 140/220 μmol/kg O_2 contours retain similar behavior). Between May and November the 1.0 Ω^e_{arag} contour reaches 30 m near-continuously over the inner shelf (i.e., from the 80 m isobath shoreward), with the exception of early October, when a strong downwelling event confines the low-Ω^e_{arag} water to the shelf-bottom (not shown). Over the outer shelf and slope, the 1.5 Ω^e_{arag} horizon shoals to less than 30 m by mid-July and the 1.0 horizon shoals to 50 m by mid-August (Figure 2). After the onset of persistent downwelling-favorable winds in mid-November the 1.0 Ω^e_{arag} and 140 μmol/kg contours retreat back to the shelf-break/slope region, similar to conditions predicted for January 2007.

[13] The coupling of low Ω_{arag} state and physically-driven upwelling dynamics would be expected, given the high DIC (low *p*H) signature associated with upwelling source waters [*Hales et al.*, 2005]. The absolute magnitude of Ω_{arag} over the coastal shelf regions, however, is largely unknown, due to a lack of depth-resolved DIC and TA measurements. This model therefore provides previously unattainable insight into both the magnitude of Ω_{arag} and how it relates to seasonal hydrography changes on the central Oregon shelf. The range in Ω^e_{arag} experienced seasonally over the shelf (e.g., 0.5–1.4 and 0.8–1.8 for the mid-shelf at 80 and 30 m, respectively) is also much greater than the uncertainty in model predictions (0.053). This favorable signal to noise ratio makes the region particularly amenable to this approach, compared to open ocean subtropical regions where the seasonal range is considerably less [*Doney et al.*, 2009].

[14] An obvious question to ask is: What is the anthropogenic contribution to Ω_{arag} on the central Oregon shelf? We used the density-anthropogenic CO_2 relationship presented by *Feely et al.* [2008a, supplement] to correct observed DIC in PNW waters for anthropogenic CO_2 input (20–40 μmol/kg) and calculated a "preindustrial" Ω^e_{arag} for our data. A parallel algorithm with the same form as equation (3) was fitted to the data (R^2 = 0.989) and used to predict the preindustrial Ω^e_{arag} = 1 horizon for the time-series data (Figure 2). This preindustrial Ω^e_{arag} = 1 threshold very closely follows the 2007 Ω^e_{arag} 0.8 isoline. Therefore, within the ability to estimate anthropogenic CO_2 content in coastal waters (±50% [*Feely et al.*, 2008a]), undersaturation over shelf/slope bottom waters is likely a natural phenomena, but an anthropogenic reduction in Ω_{arag} by 0.2 units has caused a shoaling of the 1.0 horizon by ≈25m (shelf/slope) to ≈40m (offshore). Exposure of pelagic communities to undersaturated water may therefore be lengthened or intensified by anthropogenic CO_2 input.

5. Implications

[15] The persistence of water with Ω_{arag} < 1 over the shelf throughout the May–November upwelling season has not been previously noted. Although it is unclear how organisms on the central Oregon coast are directly affected by these conditions, laboratory experiments have indicated potentially deleterious impacts for organisms exposed to waters with Ω_{arag} < 1 [*Kleypas et al.*, 2006; *Fabry et al.*, 2008; *Doney et al.*, 2009]. A clear application of the regression model presented here is to explore effects of low Ω_{arag} on shelf communities when DIC and TA data are unavailable. Preliminary examination of historical pteropod abundance data from the Oregon coast from the last 20 years (B. Peterson, unpublished data, 2009) indicates that pteropods are generally found where upwelling water is not; their abundances are maximum in offshore waters outside of the upwelling region and peak over the shelf only during winter or El Nino events, when upwelling is suppressed. In-depth examination of these data and other historical records may provide insight into adaptations organisms use to cope with low Ω_{arag} conditions.

[16] *Bakun* [1990] and *Snyder et al.* [2003] have suggested that upwelling intensity is likely to increase under future warming climate scenarios. Because the transit time of upwelling source waters from last atmospheric exposure to the sites of local upwelling are on the order of decades [*Feely et al.*, 2008a], additional anthropogenic CO_2 is already "in the pipeline" in the ocean interior, and will continue to decrease coastal Ω_{arag} well into this century, regardless of atmospheric CO_2 rise scenarios. Impacts of these changes will be better understood as studies of the seasonality in Ω_{arag} and effects on coastal organisms emerge. The Ω^e_{arag} relationship presented here (equation (3)) will need to be adjusted on 5–10 year intervals to account for the additional anthropogenic CO_2 input.

[17] A key advantage of the ability to estimate Ω_{arag} using commonly available hydrographic parameters (T, O_2) is the capability to hindcast Ω_{arag} from historical datasets to explore relationships with previously documented ecological/physical observations, provided corrections for reduced anthropogenic CO_2 in prior data, if significant, can be taken into account. For example, regression model development efforts by T. Kim et al. (Prediction of East/Japan Sea acidification over the past 40 years using a multiple-parameter regression model, submitted to *Global Biogeochemical Cycles*, 2009) highlight the importance of ventilation events for determining subsurface (50–500 m) Ω_{arag} in a 50-year hydrographic time-series in the East/Japan Sea. Continued refinement of Ω^e_{arag} regression models for the PNW and other coastal regions (Kim et al., submitted manuscript, 2009; S. R. Alin et al., manuscript in preparation, 2009) as more Ω_{arag} data become available will significantly enhance our understanding of the sensitivity of coastal regions to future CO_2-chemistry changes and warming.

[18] **Acknowledgments.** Financial support for this work was provided by NOAA Global Carbon Cycle Program Grant GC05288 to RAF, CLS, and BH. LWJ was supported by a NRC Postdoctoral Fellowship. Partial support for KL was made possible by the NRL program of KOSEF. This is NOAA/PMEL contribution 3418.

References

Anderson, L. A., and J. L. Sarmiento (1994), Redfield ratios of remineralization determined by nutrient data analysis, *Global Biogeochem. Cycles*, *8*, 65–80, doi:10.1029/93GB03318.

Bakun, A. (1990), Global climate change and intensification of coastal ocean upwelling, *Science*, *247*, 198–201, doi:10.1126/science.247.4939.198.

Doney, S. C., et al. (2009), Ocean acidification: The other CO_2 problem, *Annu. Rev. Mar. Sci.*, *1*, 169–192, doi:10.1146/annurev.marine.010908.163834.

Fabry, V. J., et al. (2008), Impacts of ocean acidification on marine fauna and ecosystem processes, *ICES J. Mar. Sci.*, *65*, 414–432, doi:10.1093/icesjms/fsn048.

Feely, R. A., et al. (2004), Impact of anthropogenic CO_2 on the $CaCO_3$ system in the oceans, *Science*, *305*, 362–366, doi:10.1126/science.1097329.

Feely, R. A., et al. (2008a), Evidence for upwelling of corrosive "acidified" water onto the continental shelf, *Science*, *320*, 1490–1492, doi:10.1126/science.1155676.

Feely, R. A., et al. (2008b), A new proxy method for estimating the aragonite saturation state of coastal waters using chemical and hydrographic Data, *Eos Trans. AGU*, *89*(53), Fall Meet. Suppl., Abstract OS33E-03.

Hales, B., T. Takahashi, and L. Bandstra (2005), Atmospheric CO_2 uptake by a coastal upwelling system, *Global Biogeochem. Cycles*, *19*, GB1009, doi:10.1029/2004GB002295.

Huyer, A., E. J. C. Sobey, and R. L. Smith (1979), The spring transition in currents over the Oregon continental shelf, *J. Geophys. Res.*, *84*, 6995–7011, doi:10.1029/JC084iC11p06995.

Kleypas, J. A., et al. (2006), Impacts of ocean acidification on coral reefs and other marine calcifiers: A guide to future research, 88 pp., Univ. Corp. of Atmos. Res., Boulder, Colo., (Available at http://www.ucar.edu/communications/Final_acidification.pdf)

Kutner, M., et al. (2004), *Applied Linear Regression Models*, McGraw-Hill, Boston, Mass.

Langdon, C., et al. (2003), Effect of elevated CO_2 on the community metabolism of an experimental coral reef, *Global Biogeochem. Cycles*, *17*(1), 1011, doi:10.1029/2002GB001941.

Lassiter, A. M., et al. (2006), Phytoplankton assemblages in the CoOP-WEST coastal upwelling area, *Deep Sea Res., Part II*, *53*, 3063–3077, doi:10.1016/j.dsr2.2006.07.013.

Lee, K., et al. (2000), Global relationships of total inorganic carbon with temperature and nitrate in surface seawater, *Global Biogeochem. Cycles*, *14*, 979–994, doi:10.1029/1998GB001087.

Lee, K., et al. (2006), Global relationships of total alkalinity with salinity and temperature in surface waters of the world's oceans, *Geophys. Res. Lett.*, *33*, L19605, doi:10.1029/2006GL027207.

Mucci, A. (1983), The solubility of calcite and aragonite in seawater at various salinities, temperatures, and one atmosphere total pressure, *Am. J. Sci.*, *283*, 780–799.

Orr, J. C., et al. (2005), Anthropogenic ocean acidification over the twenty-first century and its impact on calcifying organisms, *Nature*, *437*, 681–686, doi:10.1038/nature04095.

Park, P. K., et al. (1969), Alkalinity budget of the Columbia River, *Limnol. Oceanogr.*, *14*, 559–567.

Peterson, W. T., and J. E. Keister (2003), Interannual variability in copepod community composition at a coastal station in the northern California Current: A multivariate approach, *Deep Sea Res., Part II*, *50*, 2499–2517, doi:10.1016/S0967-0645(03)00130-9.

Sabine, C. L., and R. A. Feely (2007), The oceanic sink for carbon dioxide, in *Greenhouse Gas Sinks*, edited by D. Reay et al., pp. 31–49, CABI, Oxfordshire, U. K.

Snyder, M. A., et al. (2003), Future climate change and upwelling in the California Current, *Geophys. Res. Lett.*, *30*(15), 1823, doi:10.1029/2003GL017647.

Tunnicliffe, V., et al. (2009), Survival of mussels in extremely acidic waters on a submarine volcano, *Nat. Geosci.*, *2*, 344–348, doi:10.1038/ngeo500.

van Heuven, S., et al. (2009), MATLAB Program Developed for CO_2 System Calculations, *Rep. ORNL/CDIAC-105b*, U.S. Dep. of Energy, Oak Ridge, Tenn.

S. R. Alin, R. A. Feely, L. W. Juranek, and C. L. Sabine, Pacific Marine Environmental Laboratory, NOAA, 7600 Sand Point Way NE, Seattle, WA 98115, USA.

B. Hales, College of Oceanic and Atmospheric Sciences, Oregon State University, 104 Ocean Administration Bldg., Corvallis, OR 97331, USA.

K. Lee, School of Environmental Science and Engineering, Pohang University of Science and Technology, San 31, Hyoja-dong, Nam-gu, Pohang 790-784, South Korea.

J. Peterson, Cooperative Institute for Marine Resources Studies, Oregon State University, 2030 Marine Science Dr., Newport, OR 97365, USA.

W. T. Peterson, Northwest Fisheries Science Center, NMFS, 2030 S. Marine Science Dr., Newport, OR 97365, USA.